Journal of Metals, Materials and Minerals, 35(3), e2230, 2025

Solar radiation assisted photocatalytic degradation of Congo red using Ce doped $LaCoO_3$

Rishabh KAMAL[1], Rasmirekha PATTANAIK[1], Debapriya PRADHAN[2], and Suresh Kumar DASH[1,*]

[1] *Department of Chemistry, ITER, Siksha 'O' Anusandhan (Deemed to be University), Bhubaneswar, Odisha 751030, India*
[2] *Department of Chemistry, Centurion University of Technology and Management, Bhubaneswar, Odisha 751009, India*

***Corresponding author e-mail**: sureshdash@soa.ac.in

Received date:
16 December 2024
Revised date:
8 March 2025
Accepted date:
10 June 2025

Keywords:
Perovskite;
Ce-$LaCoO_3$;
Congo red;
Kinetic;
Solar light

Abstract

$LaCoO_3$ and cerium (Ce)-doped $LaCoO_3$ catalysts were synthesized via a sol-gel method to degrade Congo red dye under sunlight. Structural and optical analyses, including X-ray diffraction (XRD), X-ray photoelectron spectroscopy (XPS), and UV-visible spectroscopy, revealed that Ce doping reduced the material's band gap from 2.5 eV to 2.3 eV, enhancing light absorption. The doped catalyst also shifted the crystal structure from rhombohedral to cubic while maintaining lattice stability, with smaller crystallite sizes (9.30 nm vs. 10.59 nm for undoped $LaCoO_3$). Under optimized conditions (60 mg catalyst, pH 5.5, 135 min), Ce-doped $LaCoO_3$ achieved 85% dye degradation, outperforming undoped $LaCoO_3$ (77%). Hydroxyl and superoxide radicals were identified as key contributors to the degradation process, following first-order reaction kinetics. The catalyst retained 79% efficiency after five reuse cycles, demonstrating robustness. These improvements highlight Ce-doped $LaCoO_3$ as a sustainable, solar-driven solution for wastewater treatment.

1. Introduction

The rapid pace of industrial growth and economic advancement has led to severe environmental consequences. Among these, water pollution caused by toxic organic dyes has become a critical concern. The textile industry generates millions of tons of wastewater annually, releasing over 100,000 types of synthetic dyes into ecosystems. Recent studies highlight that toxic azo dyes like Congo red persist in aquatic environments, disrupting biodiversity and posing carcinogenic risks to humans through bioaccumulation [1,2,56]. For instance, [56] reports that 60% to 70% of industrial dye effluents remain untreated globally, exacerbating groundwater contamination. To address this, innovative remediation technologies such as advanced photocatalysis have gained prominence. Traditional methods like adsorption and flocculation often fail to degrade complex dye molecules completely, generating secondary sludge [3,4]. In contrast, semiconductor-based photocatalysts offer a sustainable alternative by leveraging solar energy to mineralize pollutants. Recent advances in nanostructured perovskites, particularly Ce-doped systems, demonstrate exceptional efficiency in degrading stubborn dyes like methyl orange and rhodamine B under visible light [57,58]. For example, [57] achieved 95% degradation of methylene blue using Ce-ZnO nanocomposites, while [58] highlighted the role of oxygen vacancies in enhancing ROS generation for dye breakdown. Several methods have been proposed to address these environmental challenges. These include adsorption, biodegradation, and flocculation [3], as well as ultra-filtration [4]. Advanced oxidation processes (AOPs) have also gained attention for their efficiency in contaminant removal. However, many of these methods generate secondary pollutants or face cost limitations. For instance, while AOPs are widely used, their high operational costs restrict large-scale application [5-9].

To optimize photodegradation processes, light stability testing is often employed. This involves accelerated aging experiments to simulate long-term effects of light exposure in shorter durations. Most studies focus on visible fading of dyes, but understanding the underlying degradation mechanisms is crucial for improving photocatalytic systems [10].

Nanomaterial-based photocatalysis offers a promising alternative. By harnessing solar energy, photocatalysts can generate electron-hole pairs that drive pollutant degradation [11,12]. These charge carriers produce reactive oxygen species (ROS), which break down toxic organic compounds into harmless byproducts. This approach is both sustainable and energy-efficient.

Perovskite materials, traditionally lead-based (ABO_3), are widely used in photovoltaics and catalysis. However, lead's toxicity has spurred research into safer alternatives [13]. Lead-free perovskites, such as $LaCoO_3$, retain structural stability and catalytic activity while avoiding environmental hazards [14]. Their properties can be tailored by substituting A-site or B-site cations or adjusting oxygen vacancies [15]. For example, lanthanide cations at the A-site enhance structural flexibility, while transition metals like cobalt at the B-site enable redox activity [16].

$LaCoO_3$ has shown potential in photocatalytic applications due to its optical and catalytic properties [17-23]. Despite advances in photocatalytic materials, challenges such as poor visible-light absorption, rapid charge recombination, and limited reusability persist in perovskite-based systems [24]. Cerium-doped $LaCoO_3$ offers a promising solution due to Ce's redox versatility and its ability to modify electronic structures [25,26]. However, the interplay between Ce doping, structural stability, and photocatalytic efficiency under solar light remains underexplored. By synthesizing Ce-doped $LaCoO_3$ via a scalable sol-gel method and

demonstrating 85% dye removal with robust reusability, this work provides a cost-effective, solar-driven strategy for wastewater treatment. The findings advance the design of lead-free perovskites for environmental remediation, bridging the gap between laboratory innovation and real-world application.

2. Material and synthesis methods

2.1 Precursor and chemicals

All chemicals, including lanthanum nitrate hexahydrate $La(NO_3)_3 \cdot 6H_2O$ (Loba Chemie Pvt. Ltd. 99%), cobalt nitrate hexahydrate $Co(NO_3)_2 \cdot 6H_2O$ (HiMedia Laboratories Private Limited, 99%), cerium nitrate hexahydrate $Ce(NO_3)_3 \cdot 6H_2O$ (HiMedia Laboratories Private Limited, 99%), and citric acid monohydrate $C_6H_8O_7 \cdot H_2O$, were of analytical grade and were used as received without any additional purification.

2.2 Synthesis of $LaCoO_3$ & cerium doped $LaCoO_3$ nano-structures

$LaCoO_3$ perovskite oxides and Ce-doped $LaCoO_3$ were prepared using the sol-gel technique, utilizing nitrate salts (La, Ce, and Co) as starting materials. Pure $LaCoO_3$ and Ce-doped $LaCoO_3$ were synthesized by combining stoichiometric ratios of La and Ce precursors in a 1:1 ratio. The required amounts of precursors were accurately measured and dissolved in 100 mL of deionized water. Citric acid, added in a 10% excess by weight, was introduced to act as a chelating agent. The resulting solution was heated to 80°C with continuous stirring until the chelation reaction led to the formation of a gel. This gel was dried in an oven at 100°C, ground manually, and then calcined at 600°C for 6 h. The black powders were collected once the temperature naturally cooled. Ce-doped $LaCoO_3$ nanostructures with a Ce concentration of 0.2 wt% were prepared by replacing a calculated amount of $Ce(NO_3)_3$ in the $LaCoO_3$ matrix. The synthesized nano-structures were stored in airtight sample tubes and subjected to basic characterization and photocatalytic analysis [27]. They were denoted as $LaCoO_3$ and Ce doped $LaCoO_3$.

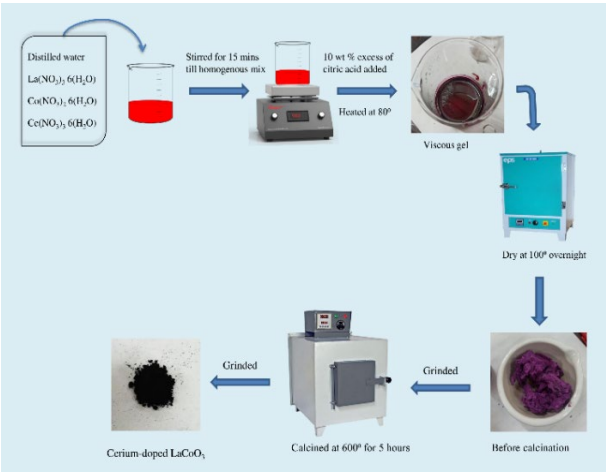

Scheme 1. Schematic diagram of synthesis of Ce-doped $LaCoO_3$.

2.3 Characterizations

The crystallinity and phase structure of the prepared samples were determined by X-ray diffraction (XRD) patterns (X-ray diffractometer-7000 from Shimadzu) using CuKα monochromatic radiation ($10° \leq 2\theta \leq 80°$), Cu Kα radiation l = 1.54 Å, at a scan rate of 2°/min. While FTIR analysis in the 4000 cm^{-1} to 400 cm^{-1} range was performed using the IRAFFINTT-2 spectrometer, Field emission scanning electron microscope (ZEISS SUPRA 55) were used to examine the surface morphology of the synthesized materials. EDS analysis was used to determine the chemical composition. The photocatalyst's optical properties were assessed using a UV-VIS spectrophotometer. Finally, the samples' electrochemical studies were evaluated using cyclic voltammetry and XPS (ESCA+ Omicron Nano Technology).

2.4 Photocatalysis studies

To evaluate the photocatalytic performance of synthesized $LaCoO_3$ and Ce-doped $LaCoO_3$ nanostructures, a stock solution of Congo red dye was prepared by dissolving 50 mg of Congo red in 1 L of deionized water, creating a 50 ppm solution. This stock solution was then diluted to obtain 1 ppm, 3 ppm, and 5 ppm concentrations for further tests. In the photocatalytic experiment, 25 mL of the 50 ppm Congo red solution was used, with varying amounts of $LaCoO_3$ and Ce-doped $LaCoO_3$ catalysts (20 mg, 40 mg, 60 mg, and 80 mg) added. The mixture was stirred in the dark for 30 min with magnetic stirring to establish adsorption–desorption equilibrium between the dye and catalyst particles. After equilibrium, the solution was exposed to solar light to initiate Congo red degradation. Experimental conditions, including pH, initial dye concentration, catalyst dosage, and stirring time, were adjusted to enhance photocatalytic efficiency. Dye degradation was measured by tracking concentration changes at λ_{max} = 498 nm using a UV-vis spectrophotometer, following sunlight exposure [28].

3. Results and discussion

3.1 Characterization of $LaCoO_3$ & Ce doped $LaCoO_3$ nanostructures

The crystalline structures of LCO and LCCO nanostructures were characterized using X-ray diffraction (XRD) in the 2θ range of 10° to 80° (Figure 1(a)). Pristine $LaCoO_3$ exhibited distinct peaks consistent with a rhombohedral structure (JCPDS file no. 01-084-0848) [29,30] with lattice parameters a = b = c = 5.3778 Å and angles α = β = γ = 60.7980°. After Ce doping, the structure shifted to a cubic phase (JCPDS file no. 01-075-0279) with lattice constants a = b = c = 3.82 Å and α = β = γ = 90°, maintaining good crystallinity with sharp peaks. The cubic phase, with its higher symmetry, provides a more uniform environment that can facilitate faster charge carrier transport and reduce the recombination rate of photogenerated electron–hole pairs. This is critical in photocatalysis, as efficient charge separation boosts the generation of reactive species that degrade the dye [67]. Structural transitions can influence defect states. A more symmetric cubic structure generally results in a more controlled defect distribution, which minimizes trap states that could otherwise serve as recombination

centers for charge carriers [68].The main perovskite peak at 32.88° confirmed structural stability post-doping, and the XRD pattern of Ce-doped $LaCoO_3$ retained all peaks of the pristine sample, with a minor secondary CeO_2 phase present [31]. The average crystallite sizes of the samples were determined using the Scherrer equation [32].

$$D = \frac{k\lambda}{\beta \cos \theta} \quad (1)$$

The crystallite size D was calculated using the Scherrer equation, where k is a shape factor (0.89), λ is the X-ray wavelength (Cu-Kα), β is the full width at half maximum (FWHM), and θ is the peak diffraction angle. The average crystallite size was found to be 10.59 nm for LCO and 9.30 nm for LCCO [69].

The FTIR spectrum of $LaCoO_3$, shown in Figure 1(b), covers a wide wave number range (4000 cm^{-1} to 500 cm^{-1}) and highlights key vibrational features. A notable absorption peak at ~1360 cm^{-1} corresponds to O–H stretching, bending, and scissoring modes from water molecules on the perovskite surface [33]. The La-Ce-Co-O network's vibrational modes produce a strong infrared band below 700 cm^{-1}, especially visible in the Ce-doped sample. Ce^{3+} substitution slightly shifts the La-O bond to higher frequencies due to Ce-O bonding. Additional metal-oxygen bond vibrations, particularly Co-O stretching and bending modes, appear below 1000 cm^{-1}, reinforcing the distinct crystalline structure of $LaCoO_3$. Overall, the FTIR analysis confirms a robust perovskite structure with characteristic Co-O bonding and minimal water contamination. The FTIR spectrum of $LaCoO_3$ shows characteristic peaks for metal-oxygen bond vibrations, particularly Co-O stretching and bending modes within the perovskite lattice. These distinctive bands confirm the presence of a stable crystalline structure consistent with $LaCoO_3$'s stoichiometric composition. Additionally, a peak around 1360 cm^{-1} indicates O-H stretching, bending, and scissoring vibrations from water molecules on the perovskite surface. Overall, the FTIR analysis confirms a well-defined perovskite structure in the synthesized $LaCoO_3$, with distinct Co-O bonding and minimal water contamination [34].

X-ray photoelectron spectroscopy (XPS) was used to analyze the valence states of elements in the newly synthesized Ce-doped $LaCoO_3$ perovskite samples. The wide-scan spectrum displayed in Figure 2 confirms the presence of La (3d), Ce (3d), Co (2p), C (1s), and O (1s) within the perovskite matrix [35,33]. Notably, a peak below 300 eV is observed, attributed to surface-bound adventitious carbon, which is commonly detected in XPS studies. Distinct peaks at 842 eV and 863 eV represent the spin-orbit splitting of La^{3+} ions at 3d5/2 and 3d3/2, confirming the presence of La in a +3 oxidation state. The Co 2p3/2 signal, around 792 eV, appears with characteristic shake-up satellites, suggesting high-spin Co ions consistent with Co^{3+} coordination within $LaCoO_3$ structures. Additional peaks at 880 eV and 899 eV correspond to Ce 3d states, indicating that Ce is present as Ce^{3+}, confirming its successful incorporation in a +3 oxidation state within the perovskite.

FE-SEM was employed to analyze the surface morphology and particle size distribution of the synthesized samples. The high-resolution FE-SEM images allow detailed examination of the material's microstructure, providing precise nanoscale characterization. Figure 3 present FE-SEM micrographs of $LaCoO_3$ at magnifications of 1 μm and 500 nm respectively. The surface morphology appears larger irregular plate like or flake or flower like structures, with relatively compact arrangement and some agglomeration [36,37]. After 'Ce 'doping the structure in Figure 4 becomes more porous with smaller particles and a granular appearance [38]. Doping with cerium appears to have more porosity or disrupted the compactness of the material, creating a rougher texture. The introduction of cerium likely increased the surface roughness and porosity, which is beneficial for catalytic applications. Increased porosity could enhance active sites availability and mass transfer during reactions. Doping with cerium might have introduced the lattice distortion s or structural defects, leading to these changes in morphology [39]. This is consistent with modifications seen in perovskites after metal doping.

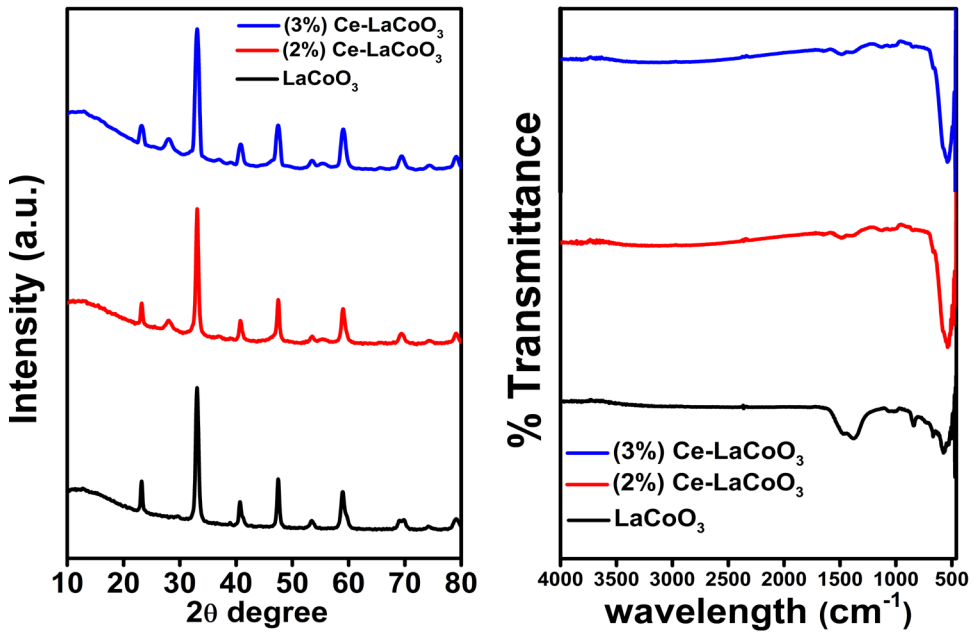

Figure 1. (a) XRD patterns, and (b) FTIR spectra of $LaCoO_3$ and Ce-doped $LaCoO_3$.

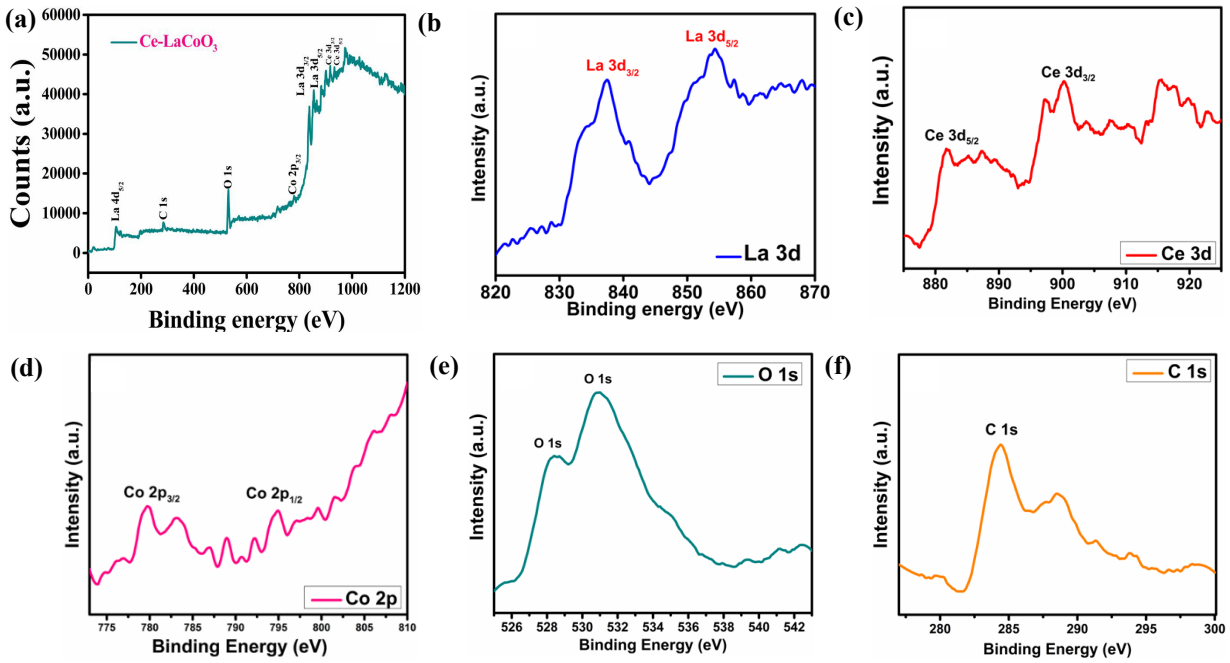

Figure 2. XPS spectra Ce doped LaCoO3 (a) survey, (b) La 3d, (c) Ce 3d, (d) Co 2p, (e) O1s, and (f) C 1s.

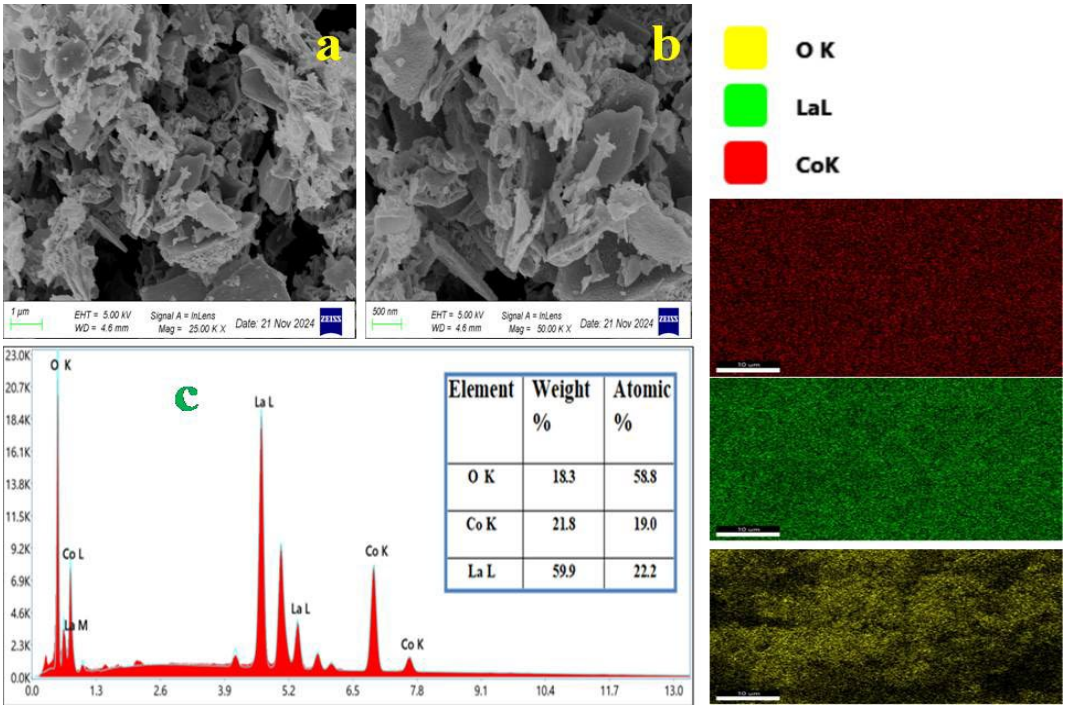

Figure 3. (a-b) FESEM images, and (c) EDAX and mapping of $LaCoO_3$.

Figure 5(a) displays the UV-DRS spectra for $LaCoO_3$ and Ce-doped $LaCoO_3$, showing notable changes in absorbance due to cerium inclusion. The undoped $LaCoO_3$ (black curve) exhibits a strong absorbance peak at 215 nm, indicating interaction with UV-vis light at that wavelength. The 2% Ce-doped $LaCoO_3$ (red curve), however, shows reduced absorbance between 215 nm and 225 nm but demonstrates a sustained increase in absorbance in the higher UV-vis range (240 nm to 300 nm) compared to the undoped material [40]. The Tauc plot in Figure 5(b) illustrates the optical band gaps of Ce-doped and undoped $LaCoO_3$, with values estimated by extrapolating the linear regions of each curve. For undoped $LaCoO_3$ (black curve), the band gap is around 2.5 eV and for 2% doped the band gap reduced to 2.3 eV and the 3% doped 2.4 eV. The reduced band gap upon Ce doping suggests that Ce ions alter the electronic structure, decreasing the energy gap between the valence and conduction bands [33,70].

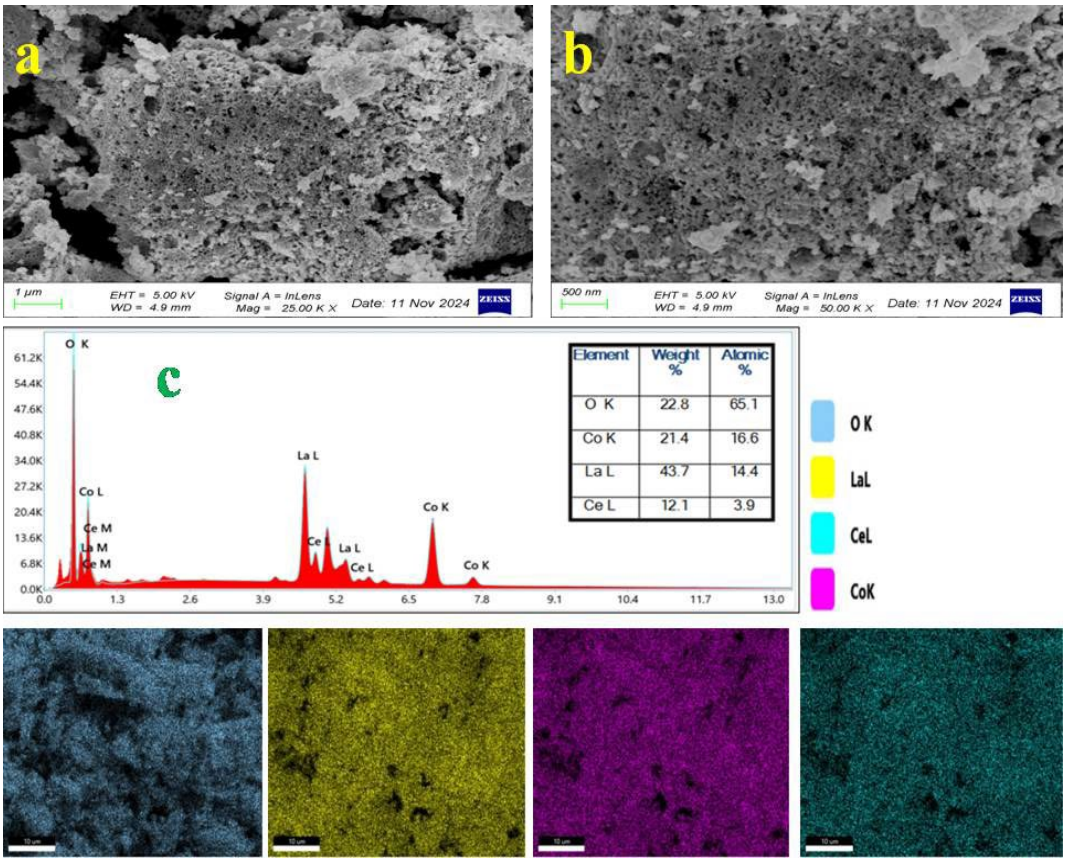

Figure 4. (a-b) FESEM images; and (c) EDAX and mapping of Ce-$LaCoO_3$.

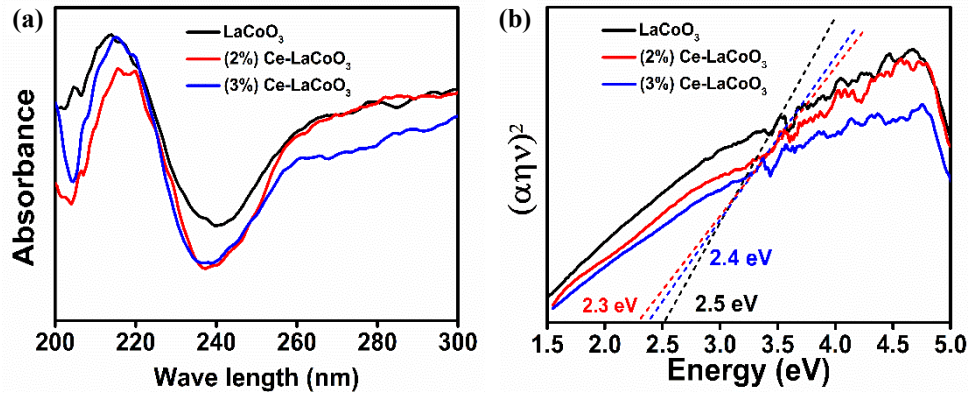

Figure 5. (a) UV-Vis absorbance spectra of $LaCoO_3$ and Ce-doped $LaCoO_3$, and (b) Tauc plot for $LaCoO_3$ and Ce-doped $LaCoO_3$.

3.2 Photocatalytic experiment

The photocatalytic efficiency of the synthesized samples was evaluated through the degradation of Congo red dye under visible light irradiation. The results of this assessment, presented below demonstrate the photocatalytic performance of $LaCoO_3$ and Ce-doped $LaCoO_3$ samples. The photocatalytic activity of the synthesized perovskite nanoparticles was assessed by examining their capacity to degrade Congo red (CR) dye under sunlight.

The photocatalytic activity of Ce-doped $LaCoO_3$ on Congo red dye is examined over duration of 135 min in Figure 6(a). The dye's initial concentration is shown by the concentration ratio (C/C_0), which is at 1.0. As time goes on, a consistent drop in C/C_0 is seen, suggesting ongoing deterioration. After 135 min, the C/C_0 ratio is almost nil, indicating almost total dye decomposition. This reduction illustrates the catalyst's potential for practical photocatalytic applications by demonstrating how well it degraded Congo red under the specified light conditions. Various concentrations of Cerium-doped $LaCoO_3$ were added to the 5 ppm CR dye solution in order to find the ideal amount of the loaded photocatalyst. The photocatalytic activity of various concentrations of Cerium-doped $LaCoO_3$ photocatalyst (20 $mg{\cdot}L^{-1}$, 40 $mg{\cdot}L^{-1}$, 60 $mg{\cdot}L^{-1}$, and 80 $mg{\cdot}L^{-1}$) put into a fixed Congo red solution is displayed in Figure 6(b). According to the photocatalytic degradation data, 60 mg of photocatalyst is the ideal level, and increasing the amount of loaded photocatalyst has a significant negative impact on the photocatalytic degradation of Congo red.

The decrease in light penetration into the dye solution caused by an excess of Ce-doped $LaCoO_3$ photocatalyst was the obvious cause of the sharp decline in the photocatalytic degradation of Congo red [41].

The pH of the dye solution is a critical parameter influencing dye degradation efficiency, as it affects electrostatic interactions between the catalyst, dye molecules, and reactive oxygen species (ROSs) during the process [42,43]. In this study, the degradation of Congo red dye, each at a concentration of 5 $mg{\cdot}L^{-1}$, was evaluated using 20 mg of Ce-doped $LaCoO_3$ nanoparticles across a pH range of 1.5 to 7.5 under solar irradiation, as illustrated in Figure 6(c). The results demonstrate that the photodegradation efficiency was optimal at pH 5.5, achieving maximum degradation within 135 min. Notably, between 80% and 57% of CR were destroyed in acidic conditions, with degradation efficiency gradually decreasing as pH rose. These nanoparticles are encircled by positively charged hydrogen ions in acidic environments, which draw in the anionic Congo red dye and promote photocatalytic destruction. The importance of acidic conditions in enhancing the photodegradation capabilities of Ce-doped $LaCoO_3$ perovskites for CR dyes removal [44].

The photocatalytic degradation efficiency of $LaCoO_3$ and Ce-doped $LaCoO_3$ was assessed at different initial concentrations of CR dye (25 ppm to 100 ppm). The findings in Figure 6(d) show that Ce-doped $LaCoO_3$ consistently outperformed $LaCoO_3$, particularly at lower dye concentrations, with the highest degradation observed at 25 ppm. The decline in efficiency at higher concentrations is likely due to reduced light penetration and limited active sites. Ce doping enhances photocatalytic activity by improving charge separation and reducing electron-hole recombination [45]. These results suggest Ce-doped $LaCoO_3$'s potential as a photocatalyst, especially in low- to moderate-concentration systems, with possible applications in wastewater treatment. To confirm the photocatalytic mechanism, control experiments were performed: (1) dye degradation under sunlight without catalyst showed negligible self-decomposition (<5%), (2) catalyst activity in dark conditions resulted only in adsorption (~12%) with no further degradation, and (3) undoped $LaCoO_3$ exhibited lower efficiency (77%) compared to Ce-doped $LaCoO_3$ (85%), emphasizing the role of Ce in enhancing charge separation [45,47]. These controls validate that the degradation is light-driven and catalyst-dependent.

Figure 7(a-b) illustrate a reduction in the absorbance of 100 mL of CR dye over time at neutral pH, with 60 mg of catalyst for CR applied for Ce doped $LaCoO_3$ over a period of 135 min. This decline in absorbance indicates the degradation of the CR dye. The degradation kinetics of CR dye (5 $mg{\cdot}L^{-1}$) under neutral conditions, using 60 mg of photocatalyst for Ce doped $LaCoO_3$, was assessed through the pseudo-first-order kinetic model. This model is represented as:

$$-\ln\left(\frac{C}{C_0}\right) = kt \tag{2}$$

Where C and C_0 are the concentrations of CR after and before the photocatalytic reaction, respectively, t is the irradiation time, and k is the rate constant [45]. The observed linear correlation between $\ln\left(\frac{C}{C_0}\right)$ and time, combined with an R^2 value nearing one, verifies that the dye degradation process follows first-order kinetics [46].

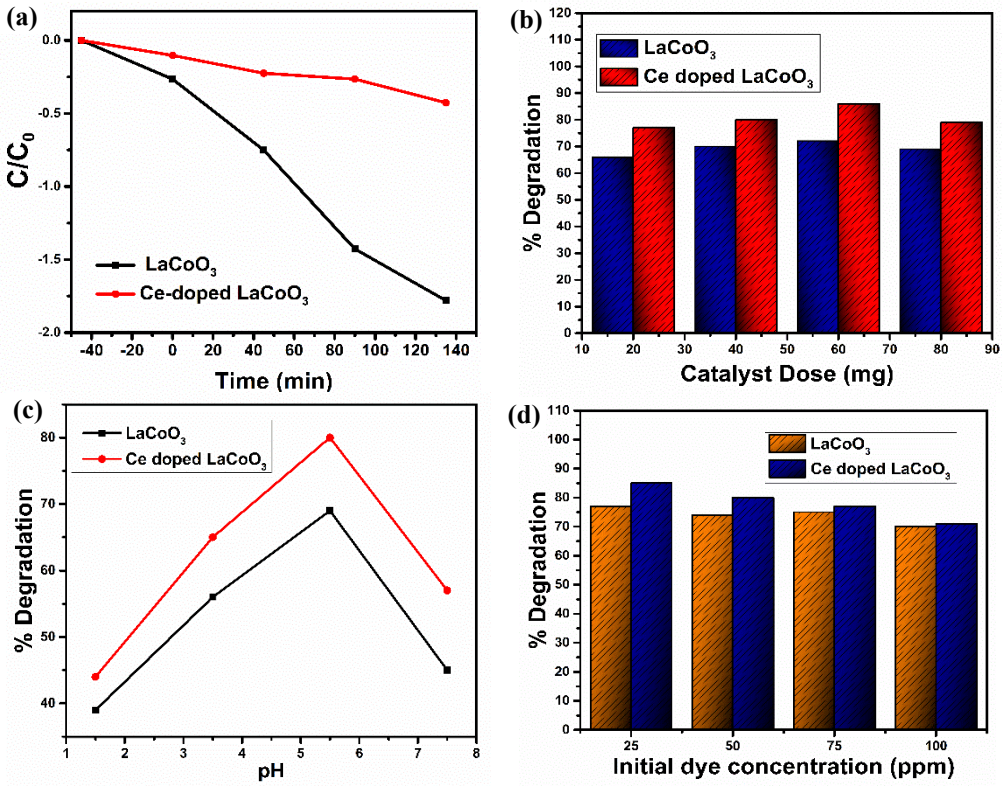

Figure 6. Photocatalytic degradation of Congo Red (CR) dye:(a) Reduction in absorbance of CR dye using Ce-doped $LaCoO_3$, (b) Effect of catalyst dosage for $LaCoO_3$ and Ce-doped $LaCoO_3$, (c) Influence of pH on dye degradation efficiency, and (d) Degradation efficiency of CR dye at different initial concentrations using $LaCoO_3$ and Ce-doped $LaCoO_3$ photocatalysts.

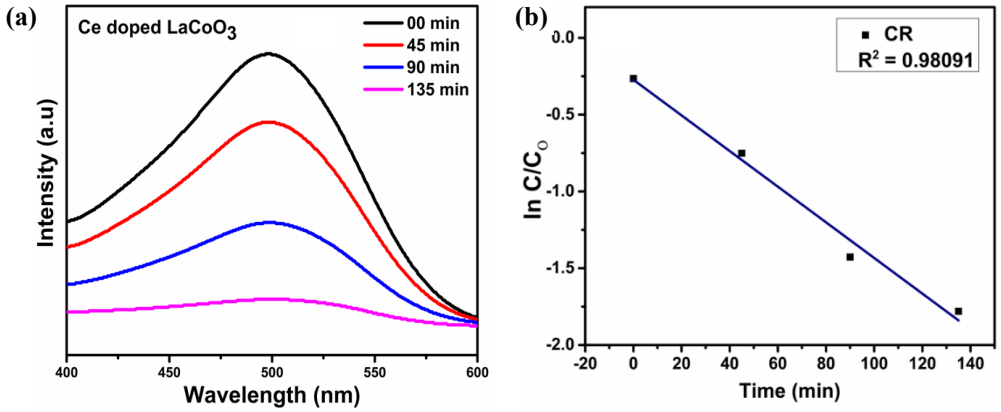

Figure 7. (a) Dye absorbance decreases with increasing illumination duration, and (b) pseudo-first-order kinetics graphic for Ce-doped $LaCoO_3$.

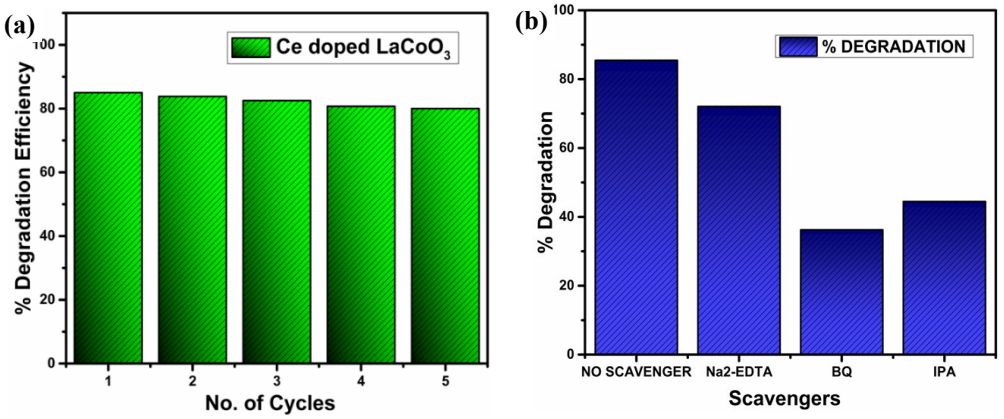

Figure 8. (a) Reusability of Ce-doped $LaCoO_3$ in successive cycles for Congo red dye degradation, and (b) Effects of scavengers on photocatalytic degradation using Ce-doped $LaCoO_3$, highlighting the roles of active species.

3.3 Mechanism, reusability and scavengers experiment

The durability of Ce-doped $LaCoO_3$ nanoparticles in degrading CR dye in Figure 8(a) was evaluated over four consecutive cycles, with efficiency levels remaining relatively stable, indicating the material's potential for repeated application. After each cycle, the catalyst was retrieved from the solution via centrifugation, followed by thorough washing and drying at 70°C. The degradation efficiency was recorded in a histogram, which illustrated a slight reduction, with effectiveness decreasing from 83% in the initial cycle to 79% by the fifth. This minor efficiency loss is likely due to the gradual reduction in catalyst mass during each recovery step [47]. The durability of Ce-doped $LaCoO_3$ nanoparticles in degrading CR dye in Figure 8(a) was evaluated over four consecutive cycles, with efficiency levels remaining relatively stable, indicating the material's potential for repeated application. After each cycle, the catalyst was retrieved from the solution via centrifugation, followed by thorough washing and drying at 70°C. The degradation efficiency was recorded in a histogram, which illustrated a slight reduction, with effectiveness decreasing from 83% in the initial cycle to 79% by the fifth. This minor efficiency loss is likely due to the gradual reduction in catalyst mass during each recovery step [47]. Nanoparticles, particularly those with smaller crystallite sizes (9.30 nm for LCCO), may escape during centrifugation or washing due to incomplete sedimentation, especially if agglomeration occurs during reuse [38]. Repeated photocatalytic cycles could induce partial sintering or pore collapse under prolonged irradiation, reducing the active surface area and accessibility of reactive sites [39,63]. Trace leaching of Ce^{3+} or Co^{3+} ions during the reaction (not quantified here) may alter the electronic structure, diminishing charge separation efficiency [31,33]. Residual dye fragments or intermediates adsorbed on the catalyst surface may block active sites, as observed in similar perovskite systems [44,49].

To mitigate mass loss and enhance recovery efficiency, the following strategies could be explored Employing ultracentrifugation or membrane filtration with smaller pore sizes could improve nanoparticle retention during separation [62]. Coating catalysts with silica or carbon layers could reduce agglomeration and improve mechanical stability during recycling [55]. Annealing used catalysts at moderate temperatures (e.g., 300°C) between cycles may decompose adsorbed contaminants and restore active sites [47]. Supporting Ce-doped $LaCoO_3$ on magnetic carriers or porous matrices (e.g., Al_2O_3) would facilitate easier recovery and minimize dispersion losses [65].

To investigate the active species involved in the photocatalytic degradation mechanism, scavenger experiments were conducted using Ce-doped $LaCoO_3$. A 5 $mg{\cdot}L^{-1}$ dye solution was prepared with 50 mg of the catalyst, and three different scavengers were introduced individually to examine their effects. Di sodium ethylenediaminetetraacetic acid (Na_2-EDTA), benzoquinone (BQ), and isopropanol (IPA) were chosen to selectively inhibit holes (h^+), superoxide radicals ($^{\bullet}O_2^-$), and hydroxyl radicals ($^{\bullet}OH$), respectively. Observations from Figure 8(b) indicate that Na_2-EDTA caused a slight decline in photocatalytic performance, while both BQ and IPA significantly reduced degradation efficiency

[48]. These results suggest that superoxide and hydroxyl radicals are critical contributors to the dye degradation process, with holes playing a less prominent role.

Scheme 2 illustrates the proposed mechanism of Degradation of CR dye with the Ce doped $LaCoO_3$ photocatalyst. When Ce-doped $LaCoO_3$ absorbs solar energy, it triggers electron movement from the valence band (VB) to the conduction band (CB), forming electron-hole pairs. Ce ions, in both +3 and +4 oxidation states, enhance charge separation, as Ce^{3+} captures electrons, preventing rapid recombination, while Ce^{4+} collects holes, improving hole availability in the VB. This coordination stabilizes electron-hole pairs and drives the generation of superoxide ($^{\bullet}O_2^-$) and hydroxyl radicals ($^{\bullet}OH$), which, along with photogenerated holes, decompose CR dye into harmless products like CO_2 and H_2O. This efficient charge transfer highlights Ce-doped $LaCoO_3$'s potential as an effective photocatalyst for dye degradation. The photocatalytic degradation of CR dye by Ce-doped $LaCoO_3$ involves several key steps. Under sunlight, Ce-$LaCoO_3$ generates electron-hole pairs as electrons move to the conduction band (CB) while holes remain in the valence band (VB). Ce ions aid charge separation: Ce^{3+} traps electrons, preventing recombination, while Ce^{4+} scavenges holes, enhancing stability. These charges generate reactive species like $^{\bullet}O_2^-$ and $^{\bullet}OH$, which degrade CR into H_2O and CO_2. This mechanism is reported to enhance photocatalytic efficiency for dye degradation [49].

$$\text{Ce doped } LaCoO_3 + h\nu \rightarrow e^-CB + h^+VB \quad (3)$$

$$e^-CB + Ce^{3+} \rightarrow Ce^{2+} \quad (4)$$

$$h^+VB + Ce^{4+} \rightarrow Ce^{3+} \quad (5)$$

$$Ce^{2+} + O_2 \rightarrow Ce^{3+} + {}^{\bullet}O_2^- \quad (6)$$

$$h^+VB + H_2O \rightarrow {}^{\bullet}OH + H^+ \quad (7)$$

$$^{\bullet}O_2^- + \text{CR dye} \rightarrow \text{Degraded products} \quad (8)$$

$$^{\bullet}OH + \text{CR dye} \rightarrow \text{Degraded products} \quad (9)$$

3.4 Implications and challenges of lead-free perovskites

The transition from lead-based perovskites (e.g., $MAPbI_3$) to lead-free alternatives (e.g., $LaCoO_3$) is pivotal for sustainable photocatalysis but introduces critical trade-offs in efficiency, stability, and scalability. Lead-based perovskites often exhibit superior visible-light absorption and charge-carrier mobility due to their narrower band gaps (~1.5 eV). For instance, $MAPbI_3$ achieves >90% degradation of methylene blue within 60 min under visible light [59]. In contrast, 2% Ce-doped $LaCoO_3$ (band gap: 2.3 eV) requires 135 min for 85% CR degradation. While $LaCoO_3$'s performance is competitive among lead-free systems, further bandgap engineering (e.g., co-doping, heterojunctions) could narrow this efficiency gap. Lead-free perovskites face stability issues under prolonged irradiation and harsh pH conditions. Although Ce-doped $LaCoO_3$ retains 79% efficiency after five cycles, lead-based counterparts like $MAPbI_3$ often degrade rapidly due to moisture sensitivity [60]. However, $LaCoO_3$'s cubic structure post-doping enhances thermal and chemical resilience, making it suitable for wastewater applications. Long-term stability (>50 cycles) and mechanistic degradation studies under real-world conditions (e.g., fluctuating pH, salinity) remain to be explored. While eliminating lead reduces toxicity risks, $LaCoO_3$ introduces lanthanum and cobalt, which pose ecological concerns if leached. Inductively coupled plasma (ICP) analyses in prior studies show minimal La^{3+}/Co^{3+} leaching (<0.5 ppm) at pH 5.5 to 7 [61], but rigorous leaching tests under acidic/alkaline conditions are warranted. Additionally, the sol-gel synthesis of $LaCoO_3$ requires high calcination temperatures (600°C), raising energy consumption concerns. Life-cycle assessments comparing lead-free and lead-based systems are critical to evaluate net environmental benefits. Scalable synthesis of $LaCoO_3$ is feasible via sol-gel methods, but doping homogeneity and nanoparticle aggregation during large-scale production need optimization. Economically, lanthanum and cobalt are costlier than lead, but their reuse potential (79% retention) offsets long-term costs. Regulatory incentives for non-toxic materials further favor lead-free perovskites in commercial adoption. In summary, while Ce-doped $LaCoO_3$ addresses lead toxicity and offers robust performance, ongoing research must optimize efficiency, validate long-term stability, and assess environmental trade-offs to position lead-free perovskites as viable, sustainable alternatives.

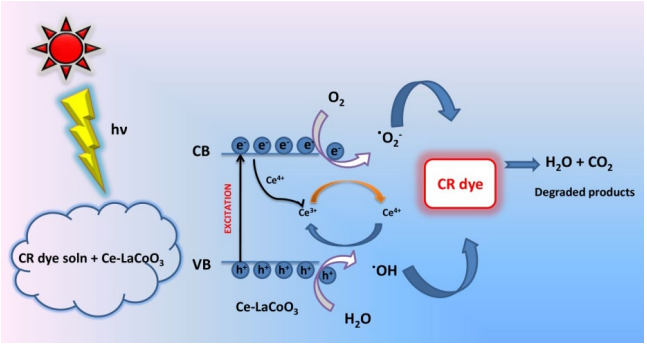

Scheme-2 Proposed mechanism for degradation of CR dye for Ce doped $LaCoO_3$

Table-1. Comparison table for doped $LaCoO_3$.

Photocatalyst	Dye	% of degradation	Time [min]	Source	Reference
$LaCoO_3/In_2O_3$	MB	~ 97	20	Visible light	[50]
$LaCoO_3/H_2O_2$	MO &MB	91 & 85	120	Visible light	[51]
$LaCoO_3$	MO	100	240	UV light	[52]
p-$LaCoO_3$/n-ZnO	Orange II	86	N.A	Visible light	[53]
Sr-Doped $LaCoO_3$	MB	88	75	Visible light	[54]
$LaCoO_3/MoS_2$	ARS, RhB	96, 90	40, 80	Visible light	[55]
Ce-doped $LaCoO_3$	CR	~ 85	135	UV-visible light	This work

3.5 Impact of synthetic conditions on photocatalytic efficiency and broader applications

3.5.1 Effect of temperature

Calcination temperature is critical in defining the crystallinity, phase formation, and dopant incorporation in perovskite photocatalysts. In our synthesis, a calcination temperature of 600°C was selected to achieve complete crystallization and uniform Ce incorporation into the $LaCoO_3$ lattice. However, literature shows that increasing calcination temperature can improve crystallinity but may also induce particle sintering, leading to larger particle sizes and a reduced surface area [62]. Conversely, lower temperatures may preserve a higher surface area but can result in incomplete phase development and a higher density of surface defects. While such defects sometimes provide additional active sites, they can also act as recombination centers that reduce photocatalytic efficiency [63]. Therefore, careful optimization of the calcination temperature is essential not only for CR degradation but also for tailoring the material for applications such as water splitting or the degradation of other organic pollutants.

3.5.2 Effect of catalyst dosage

Catalyst dosage influences both the availability of active sites and the light penetration within the reaction medium. Our results indicate that an optimal dosage (60 mg in this work) strikes a balance between providing sufficient active sites and avoiding excessive turbidity that limits photon absorption. At low dosages, the reduced number of active sites slows the degradation process, whereas excessive dosages may lead to particle agglomeration and diminished light penetration, thus hampering electron–hole pair generation [64]. This optimization is critical for achieving efficient degradation of CR and is equally relevant when applying these catalysts to other environmental remediation processes or energy conversion applications such as hydrogen production.

3.5.3 Broader implications for photocatalytic applications

The principles governing the influence of synthesis parameters are broadly applicable. Adjusting the calcination temperature and catalyst dosage allows for fine-tuning of physicochemical properties—such as surface area, defect density, and light absorption efficiency—which in turn affects charge separation and reactive oxygen species (ROS) generation. These properties are fundamental for photocatalytic processes beyond dye degradation. For example, improved charge separation is essential for advanced oxidation processes in water treatment [65] and for photocatalytic water splitting [66]. Future systematic studies that explore a broader range of synthesis conditions could further enhance the versatility of $LaCoO_3$-based photocatalysts for various environmental and energy-related applications.

4. Conclusions

According to this study, Ce-doped $LaCoO_3$ has a high potential for environmental remediation and is an efficient photocatalyst for breaking down Congo red dye when exposed to sunlight. Ce doping improves light absorption and electron-hole pair creation by decreasing the band gap from 2.5 eV to 2.3 eV. This results in an 85% degradation rate in 135 min, which is more efficient than undoped $LaCoO_3$'s 77% efficiency. While excess catalyst reduced efficiency by limiting light penetration, the ideal catalyst dosage (60 mg) and pH (about 5.5) were essential for optimizing performance. Superoxide and hydroxyl radicals were the main drivers of photodegradation, while Ce ions helped stabilize charges and minimize recombination. Tests of reusability revealed a little reduction in efficiency, demonstrating the endurance of the catalyst. The stability of the porous, crystalline shape was confirmed by structural investigations. Overall, Ce-doped $LaCoO_3$ presents a sustainable, solar-based solution for dye degradation in wastewater, supporting its potential for scalable environmental applications.

Acknowledgements

The authors extend their gratitude to the Department of Chemistry at ITER, Siksha 'O' Anusandhan (Deemed to Be University), Bhubaneswar, for providing laboratory facilities essential to this study. They also acknowledge the valuable contributions of various research institutions, particularly the Kalinga Institute of Industrial Technology and the National Institute of Technology Rourkela, for their analytical expertise.

Authors' contribution:

Rishabh Kamal conducted the experiments, collected data, prepared the manuscript, and performed material characterization. **Suresh Kumar Dash** contributed to the study's conceptualization by proposing key ideas, guiding the research, and supervising its execution. **Debapriya Pradhan** and **Rasmirekha Pattanaik** focused on data analysis.

Overall, all authors were actively involved to the fullest extent possible throughout the research process. The final manuscript was reviewed and approved by all authors.

References

[1] C. R. Holkar, A. J. Jadhav, D. V. Pinjari, N. M. Mahamuni, and A. B. Pandit, "A critical review on textile wastewater treatments: Possible approaches," *Journal of Environmental Management*, vol. 182, pp. 351-366, 2016.

[2] J. Kaushik, N. Himanshi, V. Kumar, K. M. Tripathi, and S. K. Sonkar, "Sunlight-promoted photodegradation of Congo red by cadmium-sulfide decorated graphene aerogel," *Chemosphere*, vol. 287, p. 132225, 2021.

[3] E. D. Vale-Júnior, D. R. Da Silva, A. S. Fajardo, and C. A. Martínez-Huitle, "Treatment of an azo dye effluent by peroxi-coagulation and its comparison to traditional electrochemical advanced processes," *Chemosphere*, vol. 204, pp. 548-555, 2018.

[4] J. Zhang, L. Wang, G. Zhang, Z. Wang, L. Xu, and Z. Fan, "Influence of azo dye-TiO_2 interactions on the filtration performance in a hybrid photocatalysis/ultrafiltration process," *Journal of Colloid and Interface Science*, vol. 389, no. 1, pp. 273-283, 2012.

[5] A. Azzaz, S. Jellali, H. Akrout, A. A. Assadi, and L. Bousselmi, "Optimization of a cationic dye removal by a chemically modified agriculture by-product using response surface methodology:

Biomasses characterization and adsorption properties," *Environmental Science and Pollution Research*, vol. 24, no. 11, pp. 9831-9846, 2016.

[6] A. Azzaz, S. Jellali, H. Akrout, A. A. Assadi, and L. Bousselmi, "Dynamic investigations on cationic dye desorption from chemically modified lignocellulosic material using a low-cost eluent: Dye recovery and anodic oxidation efficiencies of the desorbed solutions," *Journal of Cleaner Production*, vol. 201, pp. 28-38, 2018.

[7] S. Rashtbari, and G. Dehghan, "Biodegradation of malachite green by a novel laccase-mimicking multicopper BSA-Cu complex: Performance optimization, intermediates identification and artificial neural network modeling," *Journal of Hazardous Materials*, vol. 406, p. 124340, 2020.

[8] L. Fang, Y. Xu, L. Xu, T. Shi, X. Ma, X. Wu, Q. X. Li, and R. Hua, "Enhanced biodegradation of organophosphorus insecticides in industrial wastewater via immobilized Cupriavidus nantongensis X1T," *The Science of the Total Environment*, vol. 755, p. 142505, 2020.

[9] M. Nemiwal, T. C. Zhang, and D. Kumar, "Recent progress in g-C_3N_4, TiO_2 and ZnO based photocatalysts for dye degradation: Strategies to improve photocatalytic activity," *The Science of the Total Environment*, vol. 767, p. 144896, 2021.

[10] I. Groeneveld, M. Kanelli, F. Ariese, and M. R. Van Bommel, "Parameters that affect the photodegradation of dyes and pigments in solution and on substrate – An overview*," Dyes and Pigments*, vol. 210, p. 110999, 2022.

[11] C. Bie, H. Yu, B. Cheng, W. Ho, J. Fan, and J. Yu, "Design, fabrication, and mechanism of nitrogen-doped graphene-based photocatalyst," *Advanced Materials*, vol. 33, no. 9, 2021.

[12] Y. Zhu, J. Ren, X. Zhang, and D. Yang, "Elemental red phosphorus-based materials for photocatalytic water purification and hydrogen production," *Nanoscale*, vol. 12, no. 25, pp. 13297-13310, 2020.

[13] N. Lin, Y. Gong, R. Wang, Y. Wang, and X. Zhang, "Critical review of perovskite-based materials in advanced oxidation system for wastewater treatment: Design, applications and mechanisms," *Journal of Hazardous Materials*, vol. 424, p. 127637, 2021.

[14] Y. Tang, C. H. Mak, G. Jia, K.-C. Cheng, J-J. Kai, C.-W. Hsieh, F. Meng, W. Niu, F.-F. Li, H.-H. Shen, X. Zhu, H. M. Chen, and H.-Y. Hsu, "Lead-free hybrid perovskite photocatalysts: Surface engineering, charge-carrier behaviors, and solar-driven applications," *Journal of Materials Chemistry A*, vol. 10, no. 23, pp. 12296-12316, 2022.

[15] R. Jana, P. M. Rajaitha, S. Hajra, and H. J. Kim, "Advancements in visible-light-driven double perovskite nanoparticles for photo-degradation," *Micro and Nano Systems Letters*, vol. 11, no. 1, 2023.

[16] M. Rafiq, A. Ahmed, M. Usman, R. Ullah, F. Gao, M. Mateen, B. Yu, Y. Shen, and H. Cong "Efficient heterogeneous activation of peroxymonosulfate by manganese-doped $LaCoO_3$ perovskites for metronidazole degradation: A mechanistic study and reaction pathways," *Journal of Environmental Chemical Engineering*, vol. 11, no. 6, p. 111608, 2023.

[17] K. Ramachandran, R. Ziad, S. Columbus, K. Daoudi, J. Hammouche, M. A. El Khakani, S. Chidambaram, and M. Gaidi, "TiO_2/Si nanowires hybrid system for efficient photocatalytic degradation of organic dye," *Journal of Materials Science Materials in Electronics*, vol. 33, no. 12, pp. 9194-9203, 2021.

[18] S. Zhang, N. Han, and X. Tan, "Density functional theory calculations of atomic, electronic and thermodynamic properties of cubic $LaCoO_3$ and $La_{1-x}Sr_xCoO_3$ surfaces," *RSC Advances*, vol. 5, no. 1, pp. 760-769, 2014.

[19] A. A. Ansari, S. F. Adil, M. Alam, N. Ahmad, M. E. Assal, J. P. Labis, and A. Alwarthan, "Catalytic performance of the Ce-doped $LaCoO_3$ perovskite nanoparticles," *Scientific Reports*, vol. 10, no. 1, p. 15012, 2020.

[20] L. Predoana, B. Malic, and M. Zaharescu, "$LaCoO_3$ formation from precursors obtained by water-based sol–gel method with citric acid," *Journal of Thermal Analysis and Calorimetry*, vol. 98, no. 2, pp. 361-366, 2009.

[21] A. Ansari, V. U. Siddiqui, and W. A. Siddiqi, "4-Perovskite-type catalytic materials for water treatment," in *Hybrid Perovskite Composite Materials*, Woodhead Pulishing, 2020, pp. 117-134.

[22] J. Guo, P. Li, and Z. Yang, "A novel Z-scheme g-C_3N_4/$LaCoO_3$ heterojunction with enhanced photocatalytic activity in degradation of tetracycline hydrochloride," *Catalysis Communications*, vol. 122, pp. 63-67, 2019.

[23] L. Wang, Q. Pang, Q. Song, X. Pan, and L. Jia, "Novel microbial synthesis of Cu doped $LaCoO_3$ photocatalyst and its high efficient hydrogen production from formaldehyde solution under visible light irradiation," *Fuel*, vol. 140, pp. 267-274, 2014.

[24] A. Bodade, A. Bodade, G. N. Chaudhari, and S. M. Ghodsal, "Photocatalytic degradation of methylene blue dye over Sr doped $LaCoO_3$ nano-catalyst under sun light irradiation," *Journal of emerging technologies and innovative research*, vol. 9, no. 3, pp. 231-238, 2022.

[25] S. Jayapandi, P. Soundarrajan, S. S. Kumar, D. Lakshmi, M. D. Albaqami, M. Ouladsmane, and G. Mani, "Efficient Z-scheme $LaCoO_3$/In_2O_3 heterostructure photocatalyst for fast dye degradation under visible light irradiation," *Research on Chemical Intermediates*, vol. 48, no. 11, pp. 4419-4442, 2022.

[26] J. Qian, T. Wang, Z. Zhang, Y. Liu, J. Li, and D. Gao, "Engineered spin state in Ce doped $LaCoO_3$ with enhanced electrocatalytic activity for rechargeable Zn-Air batteries," *Nano Energy*, vol. 74, p. 104948, 2020.

[27] E. Nyamdavaa, E. Uyanga, G. Sevjidsuren, and P. Altantsog, "Preparation and characterization of cerium doped $LaCoO_3$ perovskite," *Journal of Surface Investigation X-ray Synchrotron and Neutron Techniques*, vol. 11, no. 2, pp. 366–370, 2017.

[28] P. K. Panda, R. Pattanaik, S. Mishra, D. Pradhan, and S. K. Dash, "Superior photocatalytic degradation of MB dye using $BiVO_4$ nanoparticles under solar light irradiation," *Materials Today Proceedings,* 2023.

[29] M. Islam, M.-G. Jeong, F. Ghani, and H.-G. Jung, "Micro emulsion synthesis of $LaCoO_3$ nanoparticles and their electro-chemical catalytic activity," *Journal of Electrochemical Science and Technology*, vol. 6, no. 4, pp. 121-130, 2015.

[30] D. A. Kumar, S. Selvasekarapandian, H. Nithya, J. Leiro, Y. Masuda, S-D. Kim, and S-K. Woo, "Effect of calcium doping on $LaCoO_3$ prepared by Pechini method," *Powder Technology*, vol. 235, pp. 140-147, 2012.

[31] L. Wu, X. Shi, H. Du, Q. An, Z. Li, H. Xu, and H. Ran, "Ce-doped $LaCoO_3$ film as a promising gas sensor for ethanol," *AIP Advances*, vol. 11, no. 5, p. 055305, 2021.

[32] Md. K. Alam, Md. S. Hossain, S. Tabassum, N. M. Bahadur, and S. Ahmed, "Green synthesis of nano-MgO using lemon juice for amplified photocatalytic degradation of organic pollutants," *Open Ceramics*, vol. 19, p. 100625, 2024.

[33] R. Pattanaik, R. Kamal, D. Pradhan, and S. K. Dash, "Efficacy of $BiFeO_3$ and $Bi_4Ti_3O_{12}$ towards photocatalytic degradation of MG and MB dyes: A comparative study under solar irradiation," *Journal of Metals Materials and Minerals*, vol. 35, no. 1, p e2228, 2025.

[34] S. Al-Farraj, and E. A. Abdelrahman, "Efficient photocatalytic degradation of congo red dye using facilely synthesized and characterized $MgAl_2O_4$ nanoparticles," *ACS Omega*, vol. 9, no. 4, pp. 4870-4880, 2024.

[35] R. Bortamuly, G. Konwar, P. K. Boruah, M. R. Das, D. Mahanta, and P. Saikia, "CeO_2-PANI-HCl and CeO_2-PANI-PTSA composites: Synthesis, characterization, and utilization as supercapacitor electrode materials," *Ionics*, vol. 26, no. 11, pp. 5747-5756, 2020.

[36] S. Yao, R. Zheng, R. Li, Y. Chen, X. Zhou, X. Ning, L. Zhan, and J. Luo, "$LaCoO_3$ acts as a high-efficiency co-catalyst for enhancing visible-light-driven tetracycline degradation of BiOI," *Journal of the American Ceramic Society*, vol. 103, no. 3, pp. 1709-1721, 2019.

[37] Y. Feng, K. Hu, M. Zhang, W. Ding, X. Kong, Z. Sheng, and Q. Liu, "Engineering A-site cation deficiency into $LaCoO_3$ thin sheets for improved microwave absorption performance," *Journal of Materials Science*, vol. 57, no. 1, pp. 204-216, 2022.

[38] P. Macwan, P. N. Dave, and S. Chaturvedi, "A review on nano-TiO_2 sol–gel type syntheses and its applications," *Journal of Materials Science*, vol. 46, no. 11, pp. 3669-3686, 2011.

[39] R. Schmitt, A. Nenning, Q. Kraynis, R. Korobko, A. I. Frenkel, I. Lubomirsky, S. M. Haile, and J. L. M. Rupp. "A review of defect structure and chemistry in ceria and its solid solutions," *Chemical Society Reviews*, vol. 49, no. 2, pp. 554-592, 2019.

[40] R. Wang, K. Zhang, X. Zhong, and F. Jiang, "Z-scheme $LaCoO_3$/C_3N_5 for efficient full-spectrum light-simulated solar photocatalytic hydrogen generation," *RSC Advances*, vol. 12, no. 37, pp. 24026-24036, 2022.

[41] G. Singh, M. K. Ubhi, K. Jeet, C. Singla, and M. Kaur, "A review on impacting parameters for photocatalytic degradation of organic effluents by ferrites and their nanocomposites," *Processes*, vol. 11, no. 6, p. 1727, 2023.

[42] M. Saeed, M. Muneer, A. U. Haq, and N. Akram, "Photocatalysis: an effective tool for photodegradation of dyes—a review," *Environmental Science and Pollution Research*, vol. 29, no. 1, pp. 293-311, 2021.

[43] A. Ajmal, I. Majeed, R. N. Malik, H. Idriss, and M. A. Nadeem, "Principles and mechanisms of photocatalytic dye degradation on TiO_2 based photocatalysts: a comparative overview," *RSC Advances*, vol. 4, no. 70, pp. 37003-37026, 2014.

[44] E. S. Al-Farraj, and E. A. Abdelrahman, "Efficient photocatalytic degradation of congo red dye using facilely synthesized and characterized $MgAl_2O_4$ nanoparticles," *ACS Omega*, vol. 9, no. 4, pp. 4870-4880, 2024.

[45] Y. Chen, S. Xu, C. F. Wen, H. Zhang, T. Zhang, F. Lv, Y. Yue, and Z. Bian, "Unravelling the role of free radicals in photocatalysis," *Chemistry - a European Journal*, vol. 30, no. 29, 2024.

[46] M. F. A. Messih, M. A. Ahmed, A. Soltan, and S. S. Anis, "Synthesis and characterization of novel Ag/ZnO nanoparticles for photocatalytic degradation of methylene blue under UV and solar irradiation," *Journal of Physics and Chemistry of Solids*, vol. 135, p. 109086, 2019.

[47] C. Alberoni, I. Barroso-Martin, A. Infantes-Molina, E. Rodriguez-Castellon, A. Talon, H. Zhao, S. You, A. Vomiero, and E. Moretti, "Ceria doping boosts methylene blue photodegradation in titania nanostructures," *Materials Chemistry Frontiers*, vol. 5, no. 11, pp. 4138-4152, 2021.

[48] R. Javaid, and U. Y. Qazi, "Catalytic oxidation process for the degradation of synthetic dyes: An overview," *International Journal of Environmental Research and Public Health*, vol. 16, no. 11, p. 2066, 2019

[49] Y. Chen, D. Ma, G. He, and S. Pan, "Effects of pH on the photocatalytic activity and degradation mechanism of rhodamine B over fusiform Bi photocatalysts under visible light," *Water*, vol. 16, no. 17, p. 2389, 2024.

[50] S. Irfan, Y. Shen, L. Li, Asfandiyar, S. Butt, and C.-W. Nan, "The Gadolinium (Gd^{3+}) and Tin (Sn^{4+}) Co-doped $BiFeO_3$ nanoparticles as new solar light active photocatalyst," *Scientific Reports*, vol. 7, no. 1, p. 42493, 2017.

[51] S. Jayapandi, S. Palanivel, S. S. Kumar, L. Devaraj, M. Albaqami, M. Ouladsmane, and G. Mani, "Efficient Z-scheme $LaCoO_3$/In_2O_3 heterostructure photocatalyst for fast dye degradation under visible light irradiation," *Research on Chemical Intermediates,* vol. 48, no. 11, pp. 4419-4442, 2022.

[52] M. Irshad, S. Columbus, and J. B. M. Parambath, "Enhanced photocatalytic activities of $LaCoO_3$ perovskite nanostructures for degrading cationic and anionic dyes," *Journal of Physics Conference Series*, vol. 2751, no. 1, p. 012030, 2024.

[53] X. Fu, Y. Chen, G. Q. Yu, C. Yu, H. Z. Wang, and G. De Zhang, "Preparation, characterization and photocatalysis properties of ultrafine perovskite-type $LaCoO_3$," *Advanced Materials Research*, vol. 197-198, pp. 935-942, 2011.

[54] A. Ouatizerga, G. Rekhila, S. Mirad, and M. Trari, "Characterization and application of the hetero-system $LaCoO_3$/ZnO for degradation of Orange II under solar light," *Chemical Papers*, vol. 77, no. 9, pp. 4935-4942, 2023.

[55] K. Sathiyamoorthy, A. Silambarasan, M. Navaneethan, and S. Harish, "Boosting the performance of $LaCoO_3$/MoS_2 perovskite interface for sustainable decontaminants under visible light-driven photocatalysis," *Chemosphere*, vol. 348, p. 140575, 2023.

[56] A. Khan, S. Sadiq, I. Khan, M. Humayun, G. Jiyuan, M. Usman, A. Khan, S. Khan, A. F. Alanazi, and M. Bououding, "Preparation of visible-light active MOFs-Perovskites (ZIF-67/$LaFeO_3$) nanocatalysts for exceptional CO_2 conversion, organic pollutants and antibiotics degradation," *Heliyon*, vol. 10, no. 5, p. e27378, 2024.

[57] S. Zaman, I. Khan, F.-M. Zhang, S. Khan, A. Khan, S. Khan, S. Sadiq, M. Rafiq, S. Saghir, and X.-J. Sun, "Synthesis of

mediator free hollow $BiFeO_3$ spheres/porous g-C_3N_4 Z-scheme photocatalysts for CO_2 conversion and Alizarin Red S degradation," *Materials Science in Semiconductor Processing*, vol. 162, p. 107534, 2023.

[58] S. Sadiq, I. Khan, M. Humayun, P. Wu, A. Khan, S. Khan, A. F. Alanazi, and M. Bououdina, "Synthesis of metal–organic framework-based ZIF-8@ZIF-67 nanocomposites for antibiotic decomposition and antibacterial activities," *ACS Omega,* vol. 8, no. 51, pp. 49244-49258, 2023.

[59] W. S. Yang, B.-W. Park, E. H. Jung, N. J. Jeon, Y. C. Kim, D. U. Lee, S. S. Shin, J. Seo, E. K. Kim, J. H. Noh, and S. i. Seok, "Iodide management innformamidinium-lead-halide–based perovskite layers for efficient solar cells, *Science*, vol. 356, no. 6345, pp. 1376-1379, 2017.

[60] N. Li, X. Niu, Q. Chen, and H. Zhou, "Towards commercialization: The operational stability of perovskite solar cells," *Chemical Society Reviews*, vol. 49, no. 22, pp. 8235-8286, 2020.

[61] N. Lin, Y. Gong, R. Wang, Y. Wang, and X. Zhang, "Critical review of perovskite-based materials in advanced oxidation system for wastewater treatment: Design, applications and mechanisms," *Journal of Hazardous Materials*, vol. 424, p. 127637, 2021.

[62] S. Phromma, T. Wutikhun, P. Kasamechonchung, T. Eksangsri, C. Sapcharoenkun, "Effect of calcination temperature on photocatalytic activity of synthesized TIO_2 nanoparticles via wet ball milling sol-gel method," *Applied Sciences*, vol. 10, no. 3, p. 993, 2020.

[63] M. R. Hoffmann, S. T. Martin, W. Choi, and D. W. Bahnemann, "Environmental applications of semiconductor photocatalysis," *Chemical Reviews*, vol. 95, no. 1, pp. 69-96. 1995.

[64] U. G. Akpan, and B. H. Hameed, "Parameters affecting the photocatalytic degradation of dyes using TiO_2-based photocatalysts: A review," *Journal of Hazardous Materials*, vol. 170, no. 2-3, pp. 520-529, 2009.

[65] M. N. Chong, B. Jin, C. W. K. Chow, and C.Saint, "Recent developments in photocatalytic water treatment technology: A review," *Water Research*, vol. 44, no. 10, pp. 2997-3027, 2010.

[66] M. Pera-Titus, V. García-Molina, M. A. Baños, J. Giménez, and S. Esplugas, "Degradation of chlorophenols by means of advanced oxidation processes: A general review," *Applied Catalysis B Environment and Energy*, vol. 47, no. 4, pp. 219-256, 2003.

[67] Z.-M. Chai, B.-H. Wang, Y.-X. Tan, Z.-J. Bai, J.-B. Pan, and L. Chen, "enhanced photocatalytic activity for selective oxidation of toluene over cubic–hexagonal CdS phase junctions," *Industrial & Engineering Chemistry Research*, vol. 60, no. 30, pp. 11106-11116, 2021.

[68] N. S. M. Viswanath, and W. B. Im, "Underlying dynamics of Double-Halide perovskites: unraveling structural complexity, bandgap modulation, optical, and carrier dynamics for Next-Generation optoelectronics," *ACS Applied Optical Materials*, vol. 3, no. 3, pp. 578-600, 2025.

[69] L. Huang, X. Huang, J. Yan, Y. Liu, H. Jiang, H. Zhang, J. Tang, and Q. Liu, "Research progresses on the application of perovskite in adsorption and photocatalytic removal of water pollutants. *Journal of Hazardous Materials*, vol. 442, p. 130024, 2022.

[70] P. Priyadarshini, P. Rout, S. Supriya, P. C. Kumar, and R. Naik, "Effect of CU concentration on optimizing the optical, morphological, and structural characteristics of ZNIN2S4 nanosheets for photoresponse applications," *ACS Applied Nano Materials*, vol. 7, no. 24, pp. 28131-28144, 2024.